Polym. Bull. (2010) 64:185–196
DOI 10.1007/s00289-009-0199-8

ORIGINAL PAPER

Fracture surface characteristics and impact properties of poly(butylene terephthalate)

Peihua Du · Bin Xue · Yihu Song · Shengjun Lu · Jie Yu · Qiang Zheng

Received: 21 February 2009 / Revised: 16 September 2009 / Accepted: 22 October 2009 /
Published online: 30 October 2009

Abstract In this article, the relationship between fracture surface feature and impact properties of poly(butylene terephthalate) (PBT) was investigated. The results indicated that the fracture surface morphology of notched impact specimens tested in the temperature range from 196 to 180 °C could be differentiated into brittle ($T \leq 20$ °C) and ductile appearances ($T > 20$ °C). The fracture surface roughness was characterized by surface roughness ratio (R_s) and fractal dimension (D_b). The fracture mode significantly influenced the relationship between impact strength and fracture surface roughness. When PBT fractured in a brittle mode, both the measured values of R_s and D_b could correspond to impact strength appropriately. On the contrary, when PBT fractured in a ductile mode, their relationship became not statistically significant because the area of the plastic deformation zone instead of fracture surface roughness might be the major factor influencing impact strength.

Keywords Poly(butylene terephthalate) (PBT) · Fractography · Fracture surface · Roughness · Impact strength

Introduction

Poly(butylene terephthalate) (PBT) is one of the known thermoplastics that have vast applications in automobile industry, electronics, and electrical appliances [1–10]. PBT is a strong and highly crystalline engineering plastic with excellent

P. Du · Y. Song · Q. Zheng (✉)
Department of Polymer Science and Engineering, Zhejiang University, 310027 Hangzhou, China
e-mail: zhengqiang@zju.edu.cn

P. Du · B. Xue · Y. Song · S. Lu · J. Yu (✉) · Q. Zheng
National Engineering Research Center for Compounding and Modification of Polymeric Materials, 550014 Guiyang, China
e-mail: polymerzju@126.com

comprehensive properties such as high impact strength, short mold cycles, and low molding temperature. Due to superior properties, PBT has attracted significant interest both in industry and academia. A number of studies have been conducted on the structure and properties of PBT. However, the relationship between the fracture surface morphology and toughness as well as the failure mechanisms need to be further investigated. The aim of this work was to investigate the relationship between fractography feature and impact strength of PBT.

Fractography is widely used in failure analysis to identify where the fracture originated, how it propagated, and whether it was brittle or ductile. The fracture surface represents the culmination of deformation and final separation and often provides clues to the toughness of materials. A considerable amount of information has been reported on the appearance of fracture surfaces formed by crack propagation in polymers by optical interferometry and scanning electron microscopy (SEM) [11–22]. It is found that there are several distinct patterns on fracture surfaces, such as radial striations, regularly spaced "rib" markings, irregular "mackerel" or "patch," and parabolic shape patterns. Fracture surface morphology and roughness are often related to material toughness [23–25], which have been quantitatively characterized [26–33].

In the present study, a fractographic approach was used to gain insight into how the failure mode of PBT changed with temperature. The fracture surface roughness was characterized by surface roughness ratio (R_s) and fractal dimension (D_b). The relationship between fracture surface roughness and impact strength was discussed.

Experimental

Materials

A commercially available grade of PBT (product name: S3130) produced by Yi Zheng Chem. Com., Jiangsu, China was used. The PBT was dried at 70 °C in a vacuum oven for 6 h, followed by injection molding into Izod impact specimens. Specimen geometry and dimensions used in this study are shown in Fig. 1.

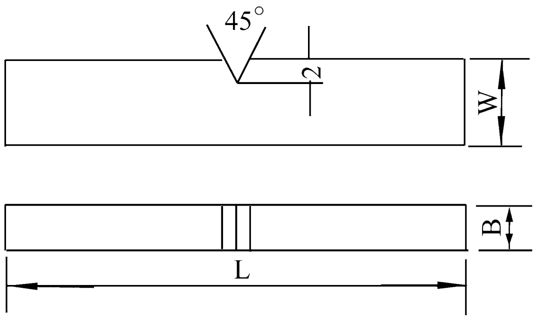

Fig. 1 Dimensions of a notched impact specimen according to GB/T1843-1996 (*Note*: $L = 80$ mm, $B = 4$ mm, $W = 10$ mm)

Impact fracture

Specimens were put in a thermostatic container for 25 min before tests. The specimens were then taken out and tested quickly. The Izod impact tests were carried out using ZBC-4B equipment. The notched specimens were subjected to the impact test in the temperature range from −196 to 180 °C. At least eight specimens for each condition were tested to reduce scattering error.

Morphological characterization

The fracture surfaces of Izod impact tested specimens were studied using a KYKY-2800B scanning electron microscope (SEM) immediately after coating gold for about 30 s to minimize electrostatic charging.

Quantitative investigation of fracture surface roughness

Measurement of R_s

Quantitative micro-measurements of fracture surface roughness were performed using the secondary electron line (SELS) method [34–39]. Here, two stereological parameters are considered useful for the characterization of fracture surface roughness [30, 34]. Profile (linear) roughness ratio, R_L, was defined as length of the profile line, L, divided by the projected length of the profile line, L_0

$$R_L = L/L_0 \quad (1)$$

Surface roughness ratio, R_s, was defined as true fracture surface area, S, divided by the apparent projected area, S_0

$$R_s = S/S_0 \quad (2)$$

Much effort has been spent on developing relationship between R_s and R_L. A linear relation commonly used is [28–30]

$$R_s = 4/\pi(R_L - 1) + 1 \quad (3)$$

It is known that the profile obtained by the SELS method is not only the presentation of the real fracture profile, but also reflects the variation of the tilt angle of the fracture surface to incident electron beam at the scanning position. The variation of the tilt angle relevant to the different positions of the fracture surface does reflect the degree of roughness of the fracture surface. Accordingly, the roughness parameter R_s measured by the SELS method can be used to characterize fracture surface roughness quantitatively.

According to previous researches [28, 36], we examined R_L from the fracture surface at a magnification of ×10, and for each fractured surface, eight scanning lines were taken along two perpendicular directions. Figure 2 shows the position for determining surface roughness ratio and Fig. 3 gives an example for a secondary electron scanning line taken from a fractured surface. Three scanning lines were

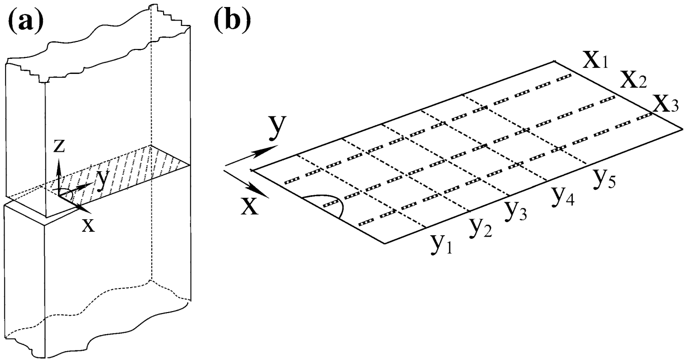

Fig. 2 **a** Sketch for the determination of the surface roughness ratio. **b** The detailed line-scanned locations on the fracture surface

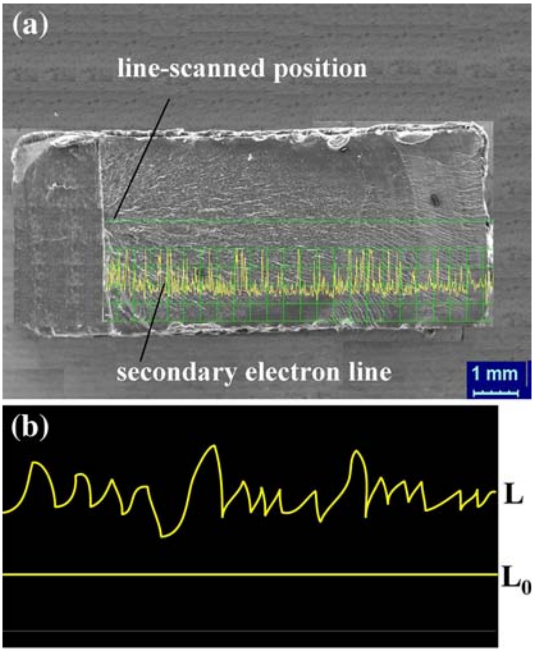

Fig. 3 **a** An example of a secondary electron scanning line taken from a fractured surface. **b** Measurement of L and L_0

taken along the y-direction: x_1 and x_3 were located 1 mm away from the edge, and x_2 passed the center of the initiation zone (as shown in Fig. 3a). Five scanning lines (y_1–y_5) were taken along the x-direction, which was 1, 2, 3, 4, and 5 mm apart from the notch individually. The micrographs of the scanning lines (as shown in Fig. 3b) were digitized with image processing software (Image Pro-plus software). The R_L value was taken as the average of the data evaluated from all the scanning lines on the same fractured surface and the R_s value was calculated from Eq. 3.

Measurement of D_b

Fractal dimension, D_b, which has been introduced to materials science as a characteristic of rough boundaries of objects, can reflect the fracture surface roughness. There are many definitions and different techniques that can be used to estimate the fractal dimension of a fracture surface or profile [27, 28, 34, 39, 40]. In this research, D_b was determined from the SEM photographs using Fractalfox software according to the box-counting method.

Results and discussion

Fractographic analysis

Figures 4, 5, 6, and 7 show SEM micrographs of the samples fractured at −40, 100, 140, and 180 °C, respectively. Figure 8 outlines different fracture modes. At low temperatures ($T \leq 20$ °C), notched PBT fractured in a brittle manner and exhibited macroscopically brittle features (Fig. 8a). Three primary zones could be defined as the initiation zone, the crack propagation zone, and the rapid fracture zone. The crack propagated from left to right on the figures. The fracture initiation zone 1 had

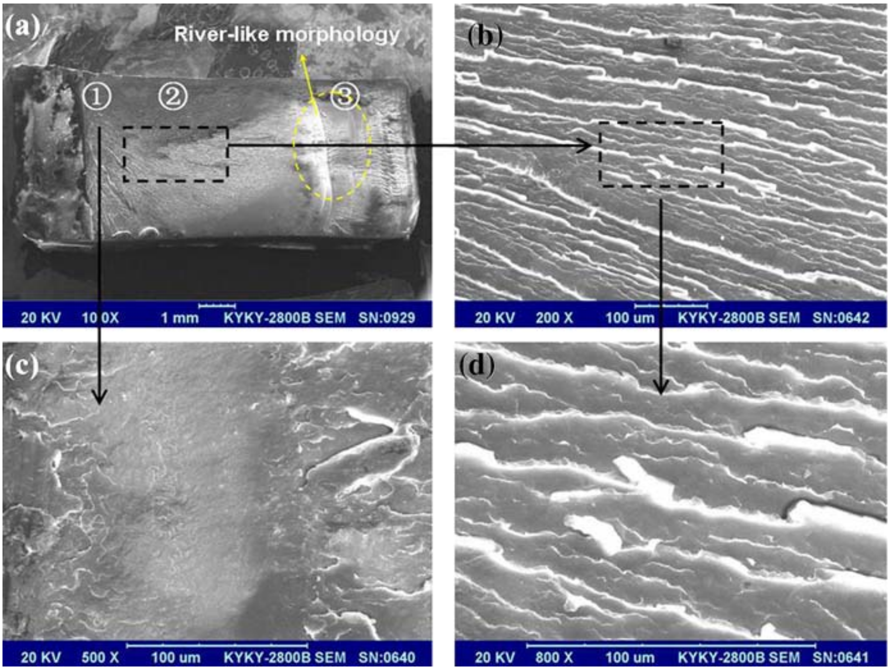

Fig. 4 Scanning electron micrographs of the fracture surface of PBT impacted tested at −40 °C. **a** The overall view of the fracture surface: 1. the initiation zone, 2. the crack propagation region, and 3. the rapid fracture zone; **b** a higher magnification of 1; **c** a higher magnification of 2; **d** a higher magnification of radial striations in (**b**)

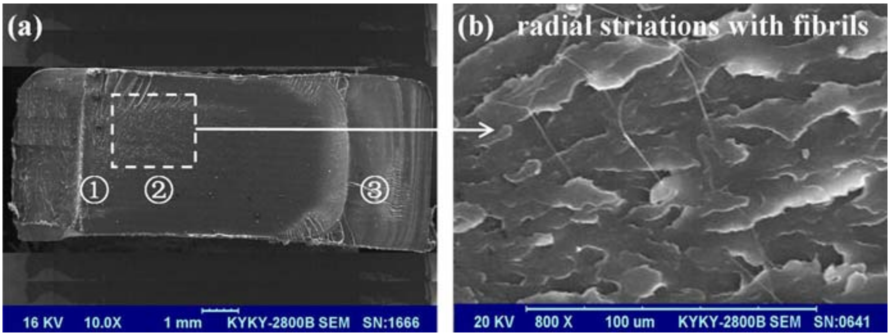

Fig. 5 Scanning electron micrographs of the fracture surface of PBT impacted tested at 100 °C: **a** the overall view of the fracture surface: 1. the initiation zone, 2. the crack propagation region, and 3. the rapid fracture zone; **b** a higher magnification of 2

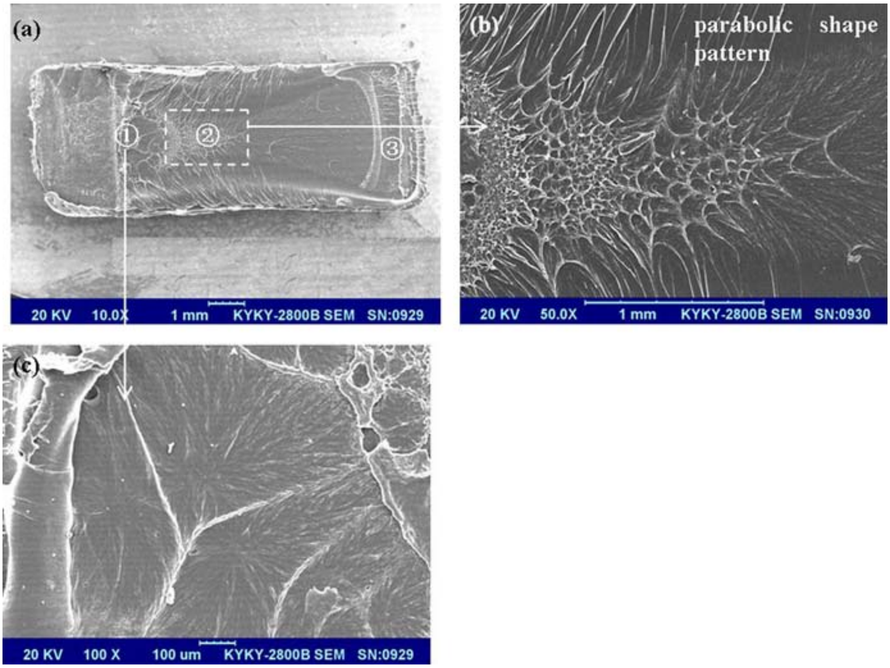

Fig. 6 Scanning electron micrographs of the fracture surface of PBT impacted tested at 140 °C. **a** The overall view of the fracture surface: 1. the initiation zone, 2. the crack propagation region, and 3. the rapid fracture zone; **b** a higher magnification of 1; **c** a higher magnification of 2

a craze-like brittle appearance (Fig. 4c). The breakdown of the craze initiation zone led to the crack propagation zone. In the crack propagation zone (Fig. 4b, d), radial lines emanated from the initiation zone in all directions. At the end of crack propagation zone there was always river-like morphologies (Fig. 4a), which corresponded to the rapid fracture zone.

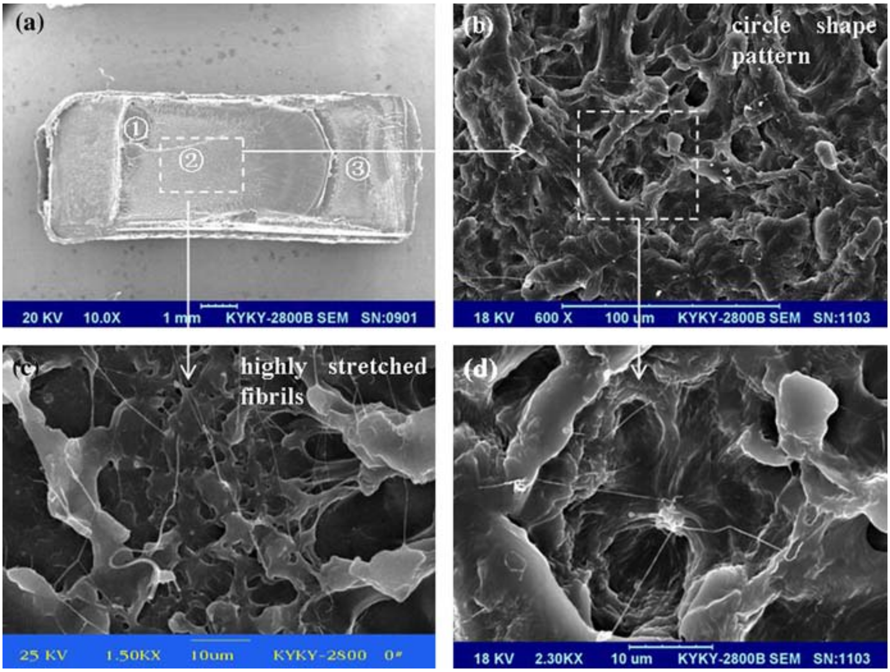

Fig. 7 Scanning electron micrographs of the fracture surface of PBT impacted tested at 180 °C. **a** The overall view of the fracture surface: 1. the initiation zone, 2. the crack propagation region, and 3. the rapid fracture zone; **b–d** a higher magnification of 2

At temperatures from 20 to 100 °C (Fig. 8b), the general fracture morphology was similar to those obtained at lower temperature ($T \leq 20$ °C), except that the overall fracture surface was smoother (Fig. 5a) and numerous curled broken fibrils could be observed on the striations in a high magnification view of the crack propagation zone (Fig. 5b), which illustrated plastic deformation produced.

As high temperatures ($T > 100$ °C), the three primary zones could still be identified. However, the fracture surface morphologies in these three zones were quite different from those at low temperatures (Fig. 8c). The size of the initiation zone increased with increasing temperature. Feeble river-like or chevron markings can be seen in Fig. 6a, c, which were highly sheared region involving tearing of presumably amorphous part of PBT. The chevron markings were characterized by shallow ridges and valleys. Existence of ductile appearance implied some much greater irreversible plastic deformation must have occurred at the crack tip leaving these residual markings on the fracture surface. The initiation zone was followed by the crack propagation zone with numerous secondary features. As temperature increased, the secondary morphology changed from parabolic to circle patterns (Figs. 6b, 7b, d), because the ratio of crack velocity to secondary crack velocity was increased [21]. Furthermore, much more highly stretched fibrils were observed (Fig. 7c). At the end of crack propagation zone there was a stick–slip line (Fig. 6a), which could be regarded as the boundary between the crack propagation zone and the rapid fracture zone.

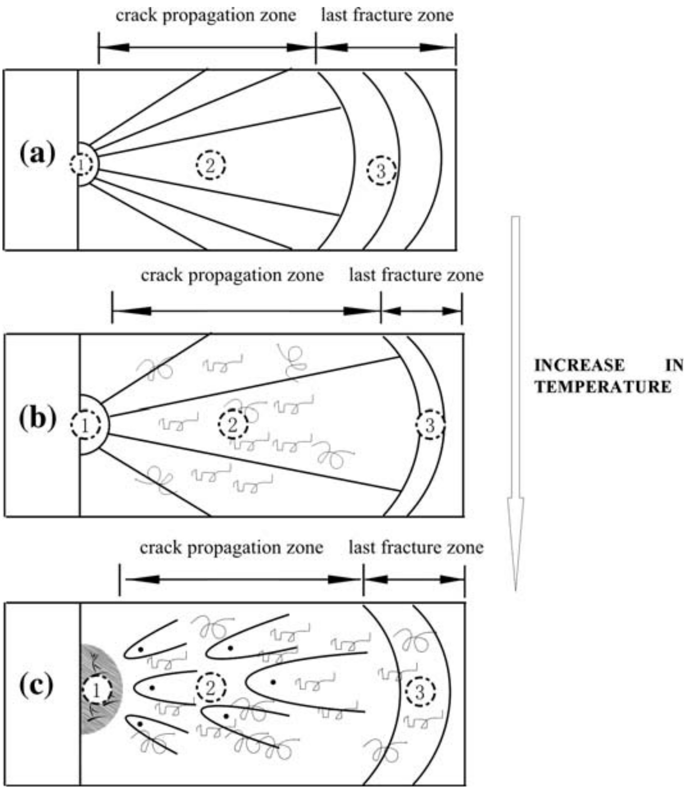

Fig. 8 Sketch for PBT fracture surface of different fracture modes showing 1. the initiation zone, 2. the crack propagation region, and 3. the rapid fracture zone. **a** Brittle fracture surface, **b** mixed mode fracture surface, and **c** ductile fracture surface

In general, fractography analysis showed that there was a transition from brittle to ductile as temperature increased. As sketched in Fig. 8, the main fracture surface morphology changed from radial lines (brittle features) to radial lines with fibrils (mixed features) and finally to secondary patterns with numerous fibrils (ductile features).

Fracture mechanism

Semicrystalline PBT is composed of crystalline and amorphous phases. When the test temperature ($T \leq 20$ °C) is below its glass transition temperature (40 °C), deformation within the amorphous phase becomes restrained. The crystals have less freedom to reorient due to the reduced mobility of the amorphous regions. The material fails by bond rupture with little plastic deformation and the fracture surface exhibits brittle features.

At temperatures near ($T > 20$ °C) and especially above the glass transition temperature, a thermally activated rearrangement may occur during the impact loading process. When temperature is further increased, the plastic deformation of the crystal blocks is encouraged. Individual crystal blocks are pulled out of the crystal ribbons and polymer chains in the amorphous zone are easily pulled into fibrils, leading to extensive stretching of the fibrils.

Relationship between impact strength and the fracture surface roughness

Values of R_s and D_b and notched Izod impact strength (σ_i) of PBT in the temperature range from −196 to 180 °C are shown in Table 1. The trend of R_s changing with temperature was similar to that of D_b. Figures 9, 10 show σ_i as a function of R_s and D_b, respectively, at low temperatures ($T \leq 20$ °C). Both figures indicate that σ_i increases with increasing fracture surface roughness (R_s and D_b). At high temperatures, plastic deformation occurred and absorbed a large amount of energy; σ_i did not show any correlation with R_s and D_b. Thus, the relationship between fracture surface roughness and impact strength was significantly influenced by the fracture mode.

The toughness of a material is generally related to the energy dissipating events that occur in the vicinity of a sharp crack [38]. The total impact energy of fracture will approximately transfer into three components: the flying energy after fracture (E_k), the initiation energy of crack (E_i), and the propagation energy of crack (E_g). According to the former study [28], σ_i can be expressed by

$$\begin{aligned}\sigma_i &= (E_k + E_i + E_g)/A = (E_k + E_i + \gamma \cdot s + \gamma_p \cdot v)/A \\ &= (E_k + E_i + \gamma \cdot AR_s + \gamma_p \cdot v)/A \end{aligned} \tag{4}$$

where A is apparent fracture surface area, γ is fracture surface energy, s is true fracture surface, γ_p is average energy of plastic deformation per unit volume, and v is volume of plastics zone.

Under the same root radius, the test temperature exercises few influence on E_i so that E_i can be considered as a constant. E_k occupies a very small proportion in the

Table 1 Values of the surface roughness parameter and impact strength at various temperatures

T (°C)	Average R_s	D_b	σ_i (kJ/m^2)
Low temperatures			
−196	15.56	1.41	3.58
−60	16.20	1.47	3.70
−40	16.25	1.66	3.89
−20	16.51	1.69	3.99
0	16.73	1.75	4.35
20	17.39	1.79	4.59
High temperatures			
60	18.83	1.89	5.92
100	10.95	1.58	8.43
140	13.95	1.67	17.88
180	16.98	1.85	14.75

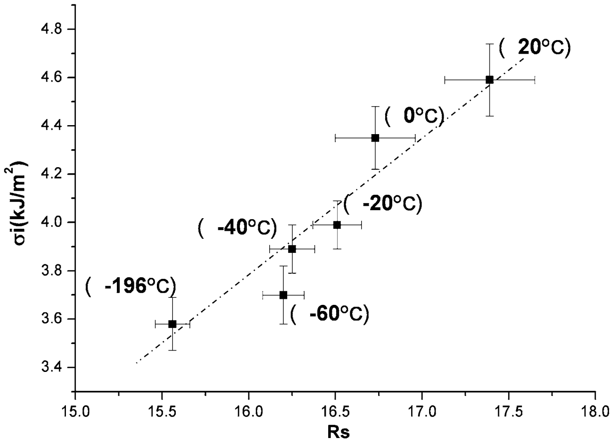

Fig. 9 Plot of impact strength versus R_s at low temperatures

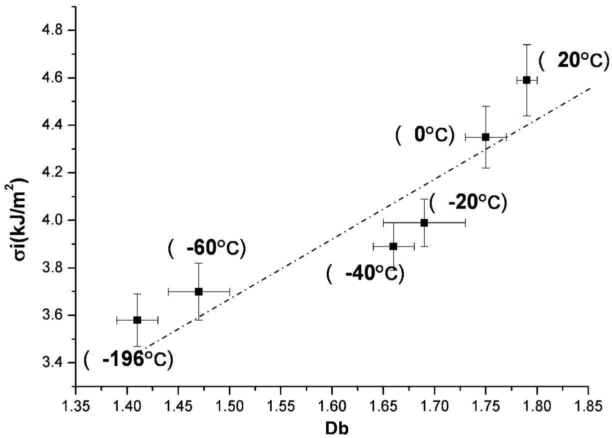

Fig. 10 Plot of impact strength versus D_b at low temperatures

total energy and it can also be considered as a constant. As a result, σ_i can be written into the specific terms

$$\sigma_i = C + \gamma \cdot R_s + \gamma_p \cdot v/A, \tag{5}$$

where C is a constant. At low temperatures ($T \leq 20$ °C), PBT fractured in a brittle manner so that v was considerably small. Equation 5 could thus be reduced to

$$\sigma_i = C + \gamma \cdot R_s \tag{6}$$

Equation 6 could well account for the increase of σ_i as a function of R_s as shown in Fig. 9.

At high temperatures ($T > 20$ °C), PBT fractured in a mixed mode or ductile mode accompanied by serious plastic deformation. A great deal of impact energy dissipated at the regions of plastic deformation as the crack propagated. Under this circumstance, the propagation energy takes a leading role in the total energy, and the initiation energy which can be considered as a constant just occupies a quite small proportion. Therefore, the variation of σ_i mainly depends on the area of plastic zone, which explains why σ_i has no correlation with R_s and D_b at high temperatures.

Conclusions

The fracture surface morphology of PBT notched impact specimens tested in the temperature range from -196 to 180 °C could be differentiated into brittle ($T \leq 20$ °C) and ductile appearances ($T > 20$ °C). Fracture mode significantly influenced impact strength σ_i as a function of R_s and D_b. When PBT fractured in a brittle mode, the measured values of R_s and D_b could correspond to the impact strength appropriately. On the contrary, when PBT fractured in a ductile mode, the relationship between σ_i and fracture surface roughness was not statistically significant, because the area of plastics deformation zone instead of fracture surface roughness became the major factor influencing impact strength.

Acknowledgments The authors gratefully acknowledge financial support for this work from Guizhou Flare Plan (No. 20008005) and Guizhou Science Fund (No. 20003072).

References

1. Volkel M (2005) Brittle fracture in PBT. Kunstst-Plast Eur 95:191–194
2. Takahashi Y, Murakami K, Nishikawa S (2002) Mechanism for the phase transition of poly(butylenes terephthalate). J Polym Sci Polym Phys 40:765–771
3. Weichenhain R, Wesner DA, Pfleging W, Horn H, Kreutz EW (1997) KrF-excimer laser pretreatment and metallization of polymers. Appl Surf Sci 110:264–269
4. Gerson LM, Leonardo BC, Elias HJ, Luiz AP (2001) Toughening of PBT by ABS, SBS and HIPS systems and the effects of reactive functionalized copolymers. Macromol Symp 176:167–180
5. Sun SL, Tan ZY, Zhou C, Zhang MY, Zhang HX (2007) Effect of ABS grafting degree and compatibilization on the properties of PBT/ABS blends. Polym Compos 28:484–492
6. Xiao JF, Hu YA, Lu HD, Cai YB, Chen ZY (2007) Effect of order of mixing on morphology and thermal properties of the compatibilized PBT and ABS alloys/OMMT nanocomposites. J Appl Polym Sci 104:2130–2139
7. Canto LB, Hage E, Pessan LA (2006) Effects of the molecular structure of impact modifier and compatibilizer on the toughening of PBT/SBS/PS-GMA blends. J Appl Polym Sci 102:5795–5807
8. Larocca NM, Hage E, Pessan LA (2005) Effect of reactive compatibilization on the properties of poly(butylene terephthalate)/acrylonitrile-ethylene-propylene-diene-styrene blends. J Polym Sci Polym Phys 43:1244–1259
9. Kelnar I, Kotek J, Munteanu BS, Kaprálková L (2004) PBT blends with rigid polymer and elastomer inclusions: the effect of component type and reactivity on mechanical behaviour. Polym Int 53:2066–2071
10. Larocca NM, Hage E, Pessan LA (2004) Toughening of poly(butylene terephthalate) by AES terpolymer. Polymer 45:5265–5277
11. Yuan Q, Misra RDK (2006) Impact fracture behavior of clay-reinforced polypropylene nanocomposites. Polymer 47:4421–4433
12. Doyle MJ (1982) Nucleation and propagation of cracks in a polystyrene craze layer. J Mater Sci 17:760–768

13. Luo WB, Yang TQ, Wang XY (2004) Time-dependent craze zone growth at a crack tip in polymer solids. Polymer 45:3519–3525
14. Cheng C, Hiltner A, Baer E, Soskey PR, Mylonakis SG (1994) Deformation of rubber-toughened polycarbonate: macroscale analysis of the damage zone. J Appl Polym Sci 52:177–193
15. Liu K, Piggott MR (1998) Fracture failure processes in polymers. I: mechanical tests and results. Polym Eng Sci 38:60–68
16. Mathew AP, Thomas S (2001) Izod impact behavior of natural rubber/polystyrene interpenetrating polymer networks. Mater Lett 50:154–163
17. Wu HY, Ma G, Xia YM (2004) Experimental study of tensile properties of PMMA at intermediate strain rate. Mater Lett 58:3681–3685
18. Lee EKC, Rudin A, Plumtree AJ (1995) The interpretation and use of fracture surface morphology—a special case for polystyrene. J Mater Sci 30:2091–2096
19. Kulawansa DM, Langford SC, Dickinson JT (1992) Scanning tunneling microscope observations of polymer fracture surfaces. J Mater Res 7:1292–1302
20. Zhang MJ, Zhi FX, Su XR (1989) Fracture toughness and crack growth mechanism for multiphase polymers. Polym Eng Sci 29:1142–1146
21. Luo WB, Yang TQ (2003) Computer simulation of conic-shaped patterns on fracture surfaces of polymers. J Appl Polym Sci 89:1722–1725
22. Kinloch AJ, Young RJ (1983) Fracture behaviour of polymers. Applied Science Publishers, London
23. Brandt A, Prokopski G (1993) On the fractal dimension of fracture surfaces of concrete elements. J Mater Sci 28:4762–4766
24. Issa MA, Hammad AM (1994) Assessment and evaluation of fractal dimension of concrete fracture surface digitized images. Cem Concr Res 24:325–334
25. Carpinteri A, Chiaia B (1995) Multifractal nature of concrete fracture surfaces and size effects on nominal fracture energy. Mater Struct 28:435–443
26. Gokhale AM, Underwood EE (1990) A general method for estimation of fracture roughness. Metall Trans A Phys Metall Mater Sci 21:1193–1199
27. Hammad AM, Issa MA (1994) Fractal dimension as a measure of roughness of concrete fracture trajectories. Adv Cem Based Mater 1:169–177
28. Yu J, Jin ZH, Lei H, Liu YC, Luo Z (1999) The quantitative relation between notched impact strength and fracture surface roughness of polymer materials. Acta Polym Sin 5:612–615
29. ElSaundani SM (1978) Profilometric analysis of fractures. Metallography 11:247–336
30. Chermant JL, Coster M (1979) Review quantitative fractography. J Mater Sci 14:509–534
31. Wright K, Karlsson B (1983) Topographic quantification of non-planar localized surfaces. J Microsc-Oxford 1:37–51
32. Underwood EE (1986) Estimating fracture characteristics by quantitative fractography. J Met 38:106–178
33. Gokhale AM, Underwood EE (1986) A new parametric roughness equation for quantitative fractography. Acta Stereol 8:43–52
34. Lech C, Andrzdj G, Joanna K (2001) On the characterization of polymer concrete fracture surface. Cem Concr Comp 23:399–403
35. Huang ZH, Tian JF, Wang ZG (1990) Study of irregular surfaces by secondary electron line scanning. Mater Sci Eng A Struct 129:1–4
36. Huang ZH, Tian JF, Wang ZG (1989) Analysis of fractal characteristics of fractured surfaces by secondary electron line scanning. Mater Sci Eng A Struct 118:19–24
37. Wang X, Zhou H, Wang ZH, Tian MS, Liu YS, Kong QP (1999) Fractal analysis of cyclic creep fractured surfaces of two high temperature alloys. Mater Sci Eng A Struct 266:250–254
38. Li XW, Tian JF, Kang Y, Su HH, Wang ZG (1996) Quantitative characterization of fracture surface roughness using secondary electron line scanning method. J Mater Sci Lett 15:2137–2140
39. Yu J, Xu T, Tian YZ, Chen XJ, Luo Z (2002) The effects of the aggregation structure parameters on impact-fractured surface fractal dimension and strain-energy release rate for polypropylene. Mater Des 23:89–95
40. Andreas S, Manfred K, Robert HS (2007) Characterization of surface activity of carbon black and its relation to polymer-filler interaction. Macromol Mater Eng 292:885–916